

Reflection and Refraction of the Laser Light Pulse at the Vacuum–Medium Interface

W Żakowicz^{1,*} and A. A. Skorupski^{2,†}

¹*Institute of Physics, Polish Academy of Sciences, Al. Lotników 32/46, 02–668 Warsaw, Poland*

²*Department of Theoretical Physics, National Centre for Nuclear Research, Hoża 69, 00–681 Warsaw, Poland*

(Dated: August 11, 2021)

By generalizing the well known results for reflection and refraction of plane waves at the vacuum–medium interface to Gaussian light beams, we obtain analytic formulas for reflection and refraction of the TM and TE laser light pulses. This enables us to give a possible explanation why no reflection was observed in light pulse photographs in some vicinity of the air–resin interface, given in L. Gao, J. Liang, C. Li, and L. V. Wang, *Nature* **516**, 74 (2014). We suggest how to modify the experimental setup so as to observe the reflected pulse.

PACS numbers: 42.25.Gy

I. INTRODUCTION

In an impressive paper [1] describing ultrafast photography (10^{11} frames per second), among examples given there was a laser light pulse photograph in some vicinity of the vacuum–resin interface, see Fig. 3(b) in [1]. The transmitted pulse could be seen there, but no reflected one was observed. Here we try to explain why there was no reflection, and how to modify the experimental setup to observe it.

In Sec. II we show that the Gaussian beams for which the transverse dimensions are constant along the beam, behave in full analogy to plane waves, and we derive formulas pertaining to their reflection and refraction at the plane vacuum–medium interface.

Section III deals with reflection and refraction of laser pulses, and Sec. IV specifies these results to the pulses used in [1] and contains the final conclusions.

We assume that in our laboratory Cartesian coordinate system (x, y, z) , with a medium at $y < 0$ and vacuum at $y > 0$, we can fulfil the boundary conditions at the interface, $y = 0$, by a superposition of three beams propagating in the x, y plane: the incident (i), reflected (r) and refracted (or transmitted, t) Gaussian beam. In the paraxial approximation, we can describe any such steady state TM beam as [2, 3] (Gaussian units)

$$H_{z_{i,r,t}} = C_{i,r,t} \exp\left(-\frac{x_{i,r,t}^2}{w_{x_{i,r,t}}^2} - \frac{z^2}{w_z^2}\right) \times \exp\{i[(ky)_{i,r,t} - \omega t]\}, \quad (1a)$$

$$E_{x_{i,r,t}} = -Z_{i,r,t} H_{z_{i,r,t}}, \quad k_{i,r,t} = \omega n_{i,r,t}/c, \quad (1b)$$

where $C_i = 1$, $C_r = R_{\text{TM}}$ is the reflection coefficient, $C_t = T_{\text{TM}}$ is the transmission coefficient, $y_{i,r,t}$ are Cartesian coordinates along each beam, $x_{i,r,t}$ are similar coordinates for transverse directions, ω is the angular frequency, c is the speed of light in vacuum, $k_{i,r,t}$ are the

wave numbers, $n_{i,r} = 1$ and $n_t = n \equiv \sqrt{\epsilon\mu}$ are the refraction indexes of vacuum and medium, $Z_{i,r} = 1$ and $Z_t = \sqrt{\mu/\epsilon}$ are similar field impedances, and the positive constants ϵ and μ characterize the medium.

Note that for each beam, the radii w_x and w_z are constant here (y independent), which requires y to be small as compared to the Rayleigh ranges \hat{y}_x and \hat{y}_z :

$$(y/\hat{y}_{x,z})^2 \ll 1, \quad \hat{y}_{x,z} = \pi w_{x,z}^2/\lambda, \quad (2)$$

where $\lambda = (c/n)2\pi/\omega$ is the wavelength.

Note that by TM (or TE) polarization we mean orthogonality of the \mathbf{H} (or \mathbf{E}) vector with respect to the plane of incidence (x, y in our case).

II. BOUNDARY CONDITIONS

In the limit $w_x \rightarrow \infty$ and $w_z \rightarrow \infty$ in (1), we obtain the plane waves: $H_z = C \exp[i(ky - \omega t)]$. Therefore in this limit, the continuity of the tangential components of \mathbf{E} and \mathbf{H} for the incident plus reflected beam versus the transmitted one at the interface ($y = 0$) implies the Snell law

$$\varphi_r = \varphi_i, \quad n \sin \varphi_t = \sin \varphi_i, \quad (3)$$

and the Fresnel formulas [3, 4] ($\nu = n \cos \varphi_t$)

$$R_{\text{TM}} = \frac{\epsilon \cos \varphi_i - \nu}{\epsilon \cos \varphi_i + \nu}, \quad T_{\text{TM}} = 1 + R_{\text{TM}}, \quad (4a)$$

$$R_{\text{TE}} = \frac{\mu \cos \varphi_i - \nu}{\mu \cos \varphi_i + \nu}, \quad T_{\text{TE}} = 1 + R_{\text{TE}}, \quad (4b)$$

where φ_i , φ_r and φ_t are the angles of incidence, reflection and refraction.

For finite radii $w_{x_{i,r,t}}$ and $w_z = w_{z_{i,r,t}}$, we have to take into account linear relations defining $x_{i,r,t}$ and $y_{i,r,t}$ as functions of the laboratory x and y ($z_{i,r,t} = -z$):

$$x_{i,r,t} = (x, y) \cdot \hat{\mathbf{x}}_{i,r,t}, \quad y_{i,r,t} = (x, y) \cdot \hat{\mathbf{y}}_{i,r,t}, \quad (5)$$

where hats denote unit vectors for local coordinate axes of each beam,

$$\hat{\mathbf{x}}_i = (\pm \cos \varphi_i, \sin \varphi_i), \quad \hat{\mathbf{x}}_t = (\cos \varphi_t, \sin \varphi_t), \quad (6)$$

* zakow@ifpan.edu.pl

† andrzej.skorupski@ncbj.gov.pl

$$\hat{y}_{i,r} = (\sin \varphi_i, \mp \cos \varphi_i), \quad \hat{y}_t = (\sin \varphi_t, -\cos \varphi_t). \quad (7)$$

At the boundary, $y = 0$, equations (5) lead to

$$\frac{x_{i,r}^2}{w_{x_{i,r}}^2} = x^2 \frac{\cos^2 \varphi_i}{w_{x_{i,r}}^2}, \quad \frac{x_t^2}{w_{x_t}^2} = x^2 \frac{\cos^2 \varphi_t}{w_{x_t}^2}. \quad (8)$$

Thus if $x = z = 0$, Eq. (1) is the same as that for plane waves, and the boundary conditions are satisfied. They will be satisfied also for nonzero x and z , if the RHSs of (8) are the same, i.e., if

$$w_{x_r} = w_{x_i}, \quad w_{x_t} = w_{x_i} \frac{\cos \varphi_t}{\cos \varphi_i} > w_{x_i}. \quad (9)$$

For the TE Gaussian beam one has to replace TM \rightarrow TE, $H_{z_{i,r,t}} \rightarrow E_{z_{i,r,t}}$, and $H_{x_{i,r,t}} = E_{z_{i,r,t}}/Z_{i,r,t}$.

III. SPECIFICATION TO LASER PULSES

If the incident laser beam is not monochromatic, but has a spectrum function $F(\omega)$, we have to include all harmonics, and the time behavior of all beams will be given by the integral (Inverse Fourier Transform)

$$\int_{-\infty}^{\infty} F(\omega) \exp(i\omega \bar{t}) d\omega \quad \text{at} \quad \bar{t} = \frac{y_{i,r,t}}{c/n_{i,r,t}} - t. \quad (10)$$

For a Gaussian spectrum function

$$F(\omega) = \exp\{ -[(\omega - \omega_0)/b]^2 \}, \quad (11)$$

centered about $\omega = \omega_0$, the Gaussian wave packets will be obtained. In that case, for a conveniently normalized TM laser beam, we end up with (neglecting the common factor $b\sqrt{\pi}$):

$$H_z(y > 0) = \exp\left[-\frac{x_i^2}{w_{x_i}^2} - \frac{(y_i - ct)^2}{w_{y_i}^2} - \frac{z^2}{w_z^2} + ik_0(y_i - ct) \right] + R_{\text{TM}} \exp\left[-\frac{x_r^2}{w_{x_r}^2} - \frac{(y_r - ct)^2}{w_{y_r}^2} - \frac{z^2}{w_z^2} + ik_0(y_r - ct) \right], \quad (12)$$

$$H_z(y \leq 0) = (1 + R_{\text{TM}}) \exp\left[-\frac{x_t^2}{w_{x_t}^2} - \frac{(y_t - ct/n)^2}{w_{y_t}^2} - \frac{z^2}{w_z^2} + ik_0n(y_t - ct/n) \right], \quad (13)$$

where

$$w_{y_i} = 2c/b, \quad w_{y_r} = w_{y_i}, \quad w_{y_t} = w_{y_i}/n, \quad (14)$$

are the the light pulse radii along each beam, while $k_0 = 2\pi/\lambda_0$, $\lambda_0 = cT_0$ and $T_0 = 2\pi/\omega_0$ are the vacuum wavenumber, wavelength and period for the beam carrier, $\omega = \omega_0$. See also (5)–(7) and (9) for remaining definitions, in which $\varphi_t = \arcsin[(\sin \varphi_i)/n]$.

Replacing $H_z \rightarrow E_z$ and $R_{\text{TM}} \rightarrow R_{\text{TE}}$ in (12) and (13), we obtain the TE beam fields.

The real parts of the complex coordinates H_z and E_z defined above give us the z coordinates of the real physical fields.

From now on, it will be convenient to work with dimensionless variables, by measuring time and space dimensions in the units of T_0 and λ_0 , see Figs. 1–4. This implies $c = 1$ and $k_0 = 2\pi$ in (12) and (13).

At $t = 0$, for each of the pulses in (12) and (13), the real part is a product of a strongly oscillating function of $y_{i,r,t}$

$[\cos(2\pi y_i), \cos(2\pi y_r), \text{ and } \cos(2\pi n y_t)]$, with wavelengths $\lambda_i = \lambda_r = 1$, $\lambda_t = 1/n$, and the envelope which is a Gaussian proportional to

$$\exp[-(\text{space coordinate}/\text{pulse radius})^2]. \quad (15)$$

During time evolution starting at some $t = t_{\text{in}} < 0$, the incident and reflected pulses move along the y_i and y_r axes with unit velocities, and the refracted pulse along the y_t axis with the velocity $1/n$.

Notice that there is a common factor $\exp(-z^2/w_z^2)$ in (12) and (13). Its square will appear as a common factor in formulas defining energy densities (time averaged over fast oscillations with $\omega = 2\omega_0$), proportional to $\mu H_z H_z^*$ and $\epsilon E_z E_z^*$. Integrating these formulas dz from $-\infty$ to ∞ we obtain (time averaged) surface energy densities, $\mathcal{E}_{\text{TM}}(x, y, t)$ and $\mathcal{E}_{\text{TE}}(x, y, t)$. Again neglecting the common factor $(w_z \sqrt{\pi}/2)$, we end up with

$$\begin{aligned} \mathcal{E}_{\text{TM}}(x, y > 0, t) = & \exp\left[-\left(\frac{x_i}{w_{x_i}/\sqrt{2}}\right)^2 - \left(\frac{y_i - t}{w_{y_i}/\sqrt{2}}\right)^2 \right] + R_{\text{TM}}^2 \exp\left[-\left(\frac{x_r}{w_{x_r}/\sqrt{2}}\right)^2 - \left(\frac{y_r - t}{w_{y_r}/\sqrt{2}}\right)^2 \right] \\ & + 2R_{\text{TM}} \exp\left[-\frac{x_i^2 + x_r^2}{w_{x_i}^2} - \frac{(y_i - t)^2 + (y_r - t)^2}{w_{y_i}^2} \right] \cos(4\pi y \cos \varphi_i), \end{aligned} \quad (16)$$

$$\mathcal{E}_{\text{TM}}(x, y \leq 0, t) = \mu(1 + R_{\text{TM}})^2 \exp\left[-\left(\frac{x_t}{w_{x_t}/\sqrt{2}}\right)^2 - \left(\frac{y_t - t/n}{w_{y_t}/\sqrt{2}}\right)^2 \right]. \quad (17)$$

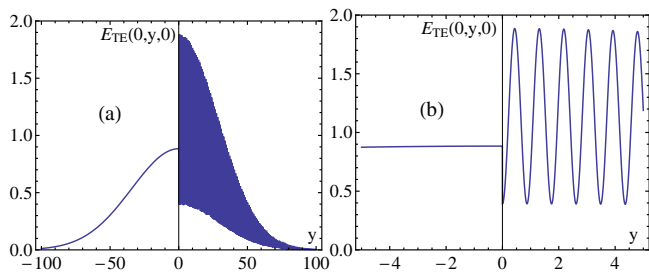


FIG. 1. (Color online) (a): $\mathcal{E}_{\text{TE}}(x=0, y, t=0)$ versus y . (b): Blowup demonstrating discontinuity in \mathcal{E}_{TE} due to discontinuity in ϵ at the interface ($y=0$), $\mathcal{E}_{\text{TE}}(y=0^-) = \epsilon \mathcal{E}_{\text{TE}}(y=0^+)$. This also demonstrates continuity of E_z at the interface.

Replacing $\text{TM} \rightarrow \text{TE}$ and $\mu \rightarrow \epsilon$ in (16) and (17) we obtain formulas for $\mathcal{E}_{\text{TE}}(x, y, t)$. The free parameters are: φ_i , w_{x_i} and w_{y_i} .

In (16) and (17), one can recognize squares of the envelopes for the fields (12) and (13), which move along the same axes and with the same velocities as the fields. The third term in (16) describes the interference of the incident and reflected pulses in vacuum. This term, different from zero when the incident and reflected pulses overlap, is strongly oscillating in the laboratory coordinate y , see Fig. 1. The wavelength (of standing wave)

$$\lambda_{\text{sw}} = \frac{1}{2 \cos \varphi_i} \quad (18)$$

depends on the angle of incidence φ_i but is independent of the pulse radii, w_{x_i} and w_{y_i} .

Note that w_{y_i} defines the laser pulse duration τ . Assuming that τ is defined as the width of the energy versus time profile at half-maximum (for incident pulse), we obtain using (16),

$$\tau = (2 \ln 2)^{1/2} w_{y_i} = 1.1774 w_{y_i}. \quad (19)$$

IV. DISCUSSION AND CONCLUSIONS

The parameters used in [1] were: $n = 1.5$ and $\mu = 1$, which implied $\epsilon = 2.25$. Furthermore, $\varphi_i = 55^\circ$ and $w_{y_i}/w_{x_i} = 2$, as we could read from Fig. 3(b) in [1]. The value of φ_i was close to the Brewster angle $\varphi_B \equiv \arctan n = 56.31^\circ$ for which $R_{\text{TM}} = 0$ [$R_{\text{TM}}^2(\varphi_i = 55^\circ) = 1.77847 \times 10^{-4}$]. This could be the reason why no reflection was observed in [1], see Fig. 2, and would suggest the laser pulse to have TM polarization. In that case, by rotating the light source by 90° around the incident beam axis, the TE polarization would be obtained, for which $R_{\text{TE}}^2(\varphi_i = 55^\circ) = 0.1393$ versus $\epsilon(1 + R_{\text{TE}})^2 = 0.8840$ for the refracted beam. The reflected pulse should then be seen along with the incident and refracted ones, see Fig. 3.

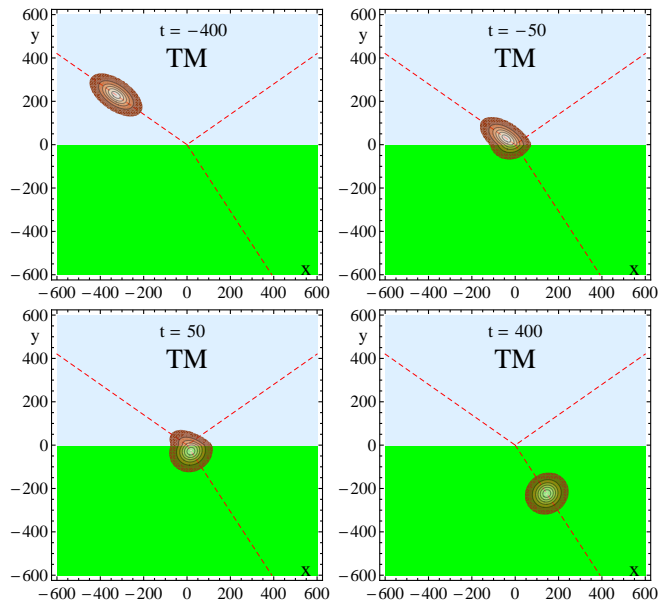


FIG. 2. (Color online) Results for $\mathcal{E}_{\text{TM}}(x, y, t)$, spatially averaged over the interference peaks, for $\epsilon = 2.25$, $\mu = 1$, $\varphi_i = 55^\circ$, $w_{x_i} = 50$, $w_{y_i} = 100$. No noticeable reflection. The pertinent videos are given in [5] (our results as above) and in [6] (experimental results of [1]).

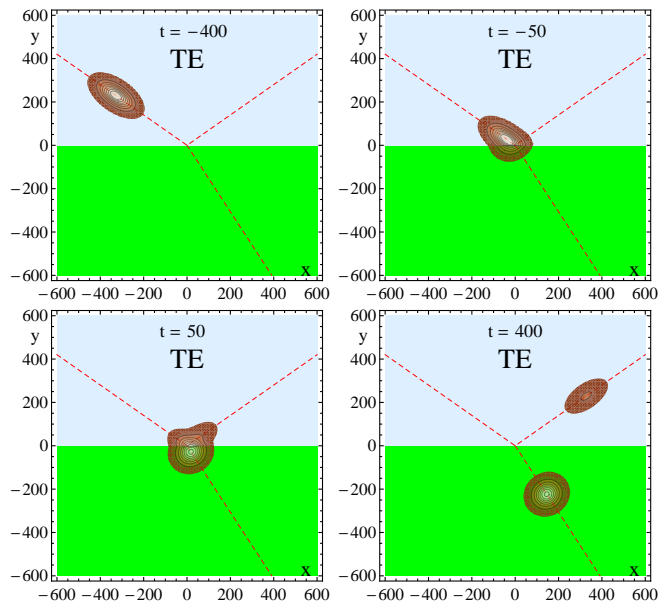


FIG. 3. (Color online) As in Fig. 2 but for $\mathcal{E}_{\text{TE}}(x, y, t)$. See [7] for the video.

In our calculations, based on the dimensionless formulas (16) and (17), for convenience we have chosen the pulse radii to be rather small: $w_{x_i} = 50$ and $w_{y_i} = 100$. The actual dimensions of the pulses used in [1] were much larger but, as we will see, the results in that case are closely related to ours.

At any instant t , the energy densities $\mathcal{E}_{\text{TM}}(x, y, t)$ and

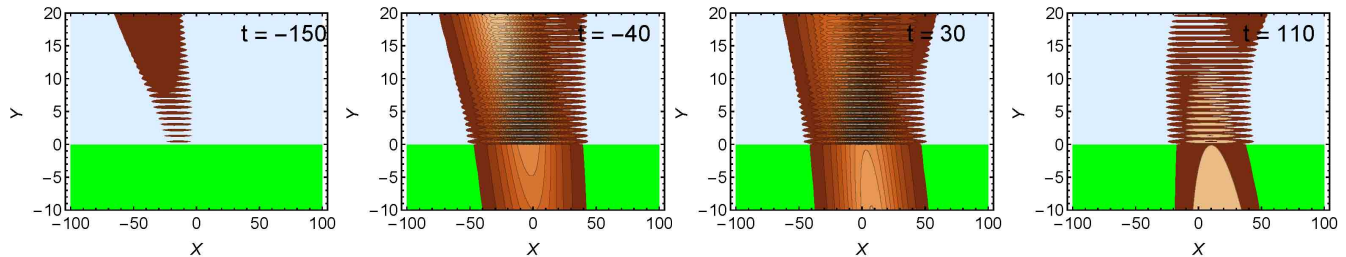


FIG. 4. (Color online) Results for $\mathcal{E}_{\text{TE}}(x, y, t)$, $w_{x_i} = 20$, and other parameters as in Fig 2.

$\mathcal{E}_{\text{TE}}(x, y, t)$ are functions of x and y . They can be represented graphically by level contours. If we multiply the pulse radii w_{x_i} and w_{y_i} by some $a > 0$, but at the same time multiply by a also x , y , and t , all exponents in (16) and (17) will remain unchanged. Therefore, if furthermore we either drop the cos term (i.e., replace it by its average value zero) or take the extreme values (± 1) of the cos, the contours in these three cases will scale along with a . For example, they will be enlarged a times if $a > 1$. During this scaling, the interference peaks shown in Fig. 1 will remain unchanged. This scaling also means that the contours in question for $a \neq 1$ will be the same as those for $a = 1$, but one has to multiply by a the numbers associated with t and with the x and y axes (the interference peaks will then get squeezed a times if $a > 1$). In particular, this scaling is applicable to the contours shown in Figs. 2 and 3, where we present “macroscopic” results (averaged over the interference peaks by neglecting the cos term).

Notice that for the incident beam, the LHS of (2) gains the factor a^{-2} if y_i and w_{x_i} are multiplied by a . This increases the accuracy of (1) if $a > 1$. In our case ($a = 1$),

$$\lambda_{\text{sw}} = 0.8717, \quad \frac{y_i^2(t = -400)}{\hat{y}_{x_i}^2} \approx 2.6 \times 10^{-3}, \quad (20)$$

and the applicability condition (2) implies $a_{\text{min}} \simeq 0.1$ ($w_{x_i \text{min}} \simeq 5$).

The laser used in [1] was characterized by the wavelength $\lambda_0 = 532$ nm and the pulse duration $\tau = 7$ ps. Dividing this τ by $T_0 = 177.33 \times 10^{-5}$ ps to make it di-

mensionless and using (19) we obtain $w_{y_i} = 3352.7$. This leads to $a = w_{y_i}/100 \simeq 33.5$, a number by which one has to multiply all numerical values in Figs. 2 and 3, to make them applicable to the experiment described in [1].

In Fig. 4 we present the details of the interference peaks evolution. The distance λ_{sw} between the peaks is given by (18) and (20).

A strong validity test for our formulas and calculations was a numerically confirmed continuity of the tangential components of \mathbf{E} and \mathbf{H} across the boundary ($y = 0^\pm$), and the fact that the total energy was conserved (time independent):

$$\int_{-1000}^{1000} dx \int_{-1000}^{1000} dy \mathcal{E}_{\text{TM}}(x, y, t) = 7853.982, \quad (21)$$

for any $t \in [-400, 400]$, and exactly the same result for $\mathcal{E}_{\text{TE}}(x, y, t)$, see Figs. 2 and 3. Incidentally, this conservation was also valid for \mathcal{E}_{TM} and \mathcal{E}_{TE} spatially averaged over the interference peaks, which can thus be treated as macroscopic energy densities. Equation (21) illustrates high accuracy of the paraxial approximation in our application.

All calculations, figures, and videos were done by using *Mathematica*.

ACKNOWLEDGMENTS

The authors would like to thank E. Infeld, M. Rusek, S. Suckewer, and P. Ziń for useful discussions.

[1] L. Gao, J. Liang, C. Li, and L. V. Wang, *Nature* **516**, 74 (2014).
 [2] P. F. Goldsmith, *Quasioptical systems: Gaussian beam, quasioptical propagation and applications* (IEEE Press/Chapman and Hall Publishers Series on Microwave Technology and RF, New York, 1998) Chap. 2.
 [3] F. Scheck, *Classical Field Theory* (Springer, Heidelberg, Dordrecht, London, New York, 2012) Chap. 4.

[4] J. D. Jackson, *Classical Electrodynamics*, 3rd ed. (Wiley, New York, 1999) Chap. 7.
 [5] See Supplemental Material at TM for the \mathcal{E}_{TM} video.
 [6] L. Gao, J. Liang, C. Li, and L. V. Wang, “Single-shot compressed ultrafast photography at one hundred billion frames per second,” (2014).
 [7] See Supplemental Material at TE for the \mathcal{E}_{TE} video.